Shah *et al. Journal of Orthopaedic Surgery and Research* (2025) 20:370
https://doi.org/10.1186/s13018-025-05773-5

Journal of Orthopaedic Surgery and Research

RESEARCH

Open Access

Functional morphology of trabecular system in human proximal femur: a perspective from P45 sectional plastination and 3D reconstruction finite element analysis

M. Adeel Alam Shah[1†], Shu-Jun Lü[1†], Jian-Fei Zhang[1], Jia-Wei Wang[1], Wei Tang[1], Wen-Chao Luo[1], Hua-Xun Lai[1], Sheng-Bo Yu[1*] and Hong-Jin Sui[1*]

Abstract

Background The trabecular architecture of proximal femur plays a crucial role in hip stability and load distribution and is often ignored in hip fracture fixation due to limited anatomical knowledge. This study analyses trabecular morphology and stress distribution, aiming to provide an anatomical foundation for optimising implant designs.

Materials and methods Twenty-one formalin-fixed human pelvises (twelve male, nine female) were prepared using P45 sectional plastination. They were sliced into 3 mm sections in the coronal, sagittal, and horizontal planes and then photographed. A 3D femur model was created from computed tomographic scans and analysed for finite element analysis (FEA) using Mimics, 3-matics, and Abaqus software to simulate static and dynamic loads, visualising stress paths for compressive and tensile regions and identifying fracture-vulnerable zones.

Results Two main trabecular systems were identified: the medial and lateral systems. The medial system includes a primary vertical trabecular group extending from the femoral shaft's medial calcar to the head and two primary horizontal groups arching from the lateral shaft, greater trochanter, and femoral neck's anterolateral and posterolateral walls toward the medial side, intersecting with the primary vertical group in the head. Secondary vertical group intersects with secondary horizontal group at the neck-trochanteric junction to form the lateral system. FEA showed peak compressive stress along the vertical groups, calcar, and medial cortex, and tensile stress along the horizontal groups, greater trochanter, and lateral cortex, creating balanced support that stabilises the femoral neck and shaft.

Conclusion The strength of proximal femur depends on dense cortical bone, calcar femorale, lateral and medial trabecular systems, and greater trochanter. While anterolateral and posterolateral areas of femoral neck and intertrochanteric regions are potential weak zones. Trabecular pattern follows stress paths, optimising load

[†]M. Adeel Alam Shah and Shu-Jun Lü contributed equally to this work.

*Correspondence:
Sheng-Bo Yu
yushengbo86@dmu.edu.cn
Hong-Jin Sui
suihj@hotmail.com

Full list of author information is available at the end of the article

distribution. These insights aid in designing robotic and bionic implants that mimic natural stress patterns, reducing complications.

Keywords Bionics, Biomechanics, Cancellous bone, Femur, Hip fracture, Sectional anatomy

Background

Hip fracture is a major orthopaedic challenge, especially for osteoporotic patients, leading to deteriorated health, mobility, and reduced life expectancy [1, 2]. Standard surgical treatments, such as internal fixation and bionic implants, often face complications due to poor integration with trabecular bone [3, 4]. This can lead to implant loosening and stress shielding, which further compromise recovery and necessitate reoperations [2, 5]. Therefore, a precise understanding of trabecular architecture and stress distribution is essential to refine implant designs and minimise complications.

The proximal femur consists of an outer cortex and inner cancellous bone. Within the cancellous bone, a complex trabecular network of bone plates plays a critical role in weight-bearing and locomotion [6, 7]. This network comprises vertical and horizontal groups that intersect at specific angles and distances, enhancing the bone's structural integrity [2]. The primary trabecular network forms radiolucent Ward's triangle in the femoral neck, while secondary trabeculae are located in the trochanters for added support [8]. Generally, during bipedal stance, the total body weight is evenly distributed across each hip joint, mainly in the form of compressive and tensile forces [1, 9, 10]. The femoral neck's vertical group absorbs compressive forces during standing and walking [9–11], while the function of the horizontal group remains less understood [7].

Wolff's law and the trajectorial theory describe that trabecular bone aligns with stress lines, adapting to tension and compression [12, 13]. However, comparative studies suggest that surrounding cortical bone and soft tissues contribute significantly to load-sharing, and trabecular adaptations may not solely reflect simple stress patterns [14–16]. Furthermore, Hammer [7] proposed that horizontal trabeculae are mainly responsible for the conduction of compression forces, rather than tension forces. Skuban et al. [11], concluded that the greater trochanter is primarily exposed to compressive forces, rather than the tensile forces previously hypothesised. Biomechanical studies on the proximal femur demonstrate that trabecular structure is influenced by principal stress trajectories, supporting Wolff's law [6, 14, 16]. In response to the increased ground reaction force and the attachment surface of the gluteus maximus, the proximal femoral diaphysis develops a reinforced mechanism that enhances muscle contraction efficiency [17]. However, loading conditions are dynamic and highly variable, and trabecular characteristics, such as density and distribution, also vary significantly. These variations are observed in both postmenopausal women and physically active individuals [5, 18, 19].

Therefore, there is no simple statement that can explain the load distribution within trabeculae. Currently, the only available modalities to study trabecular structures are radiological imaging, histology and direct dissection of the bone [7, 11, 15, 20–23]. These methods have some limitations in exploring the exact pattern, extent, and relationship with surrounding structures. Thus, a comprehensive understanding of the trabecular system in terms of morphology and load-bearing function is required for improving surgical outcomes.

To address this gap, the current study utilised the P45 sectional plastination technique and 3D reconstruction-based finite element analysis (FEA) to visualise and analyse trabecular morphology and biomechanical function in detail. The P45 sectional plastination is a polyester-based method that preserves the precise biological structure of the proximal femur resembling its living state, providing clear visual details in a transparent form [24, 25], while 3D reconstruction-based FEA offers insights into stress distribution within the bone during static and dynamic conditions [2, 10]. The main aim of this study is to accurately define the anatomy and identify areas of compression and tension within trabecular groups in a simplified manner. This will ultimately provide an anatomical foundation to optimise surgical techniques and implant compatibility with the trabecular network, potentially reducing complications and improving patient recovery.

Materials and methods

This study complies with the Declaration of Helsinki and was approved by the Biomedical Ethics Committee of Dalian Medical University, China (Approval Letter: 2023-004). Twenty-one formalin-fixed human pelvises (twelve male, nine female) were provided by the Department of Anatomy, with no history of hip joint surgery. The causes of death were myocardial infarction (57.1%), cerebrovascular accidents (28.5%), and chronic metabolic diseases (14.2%). The cadavers had a mean age of 62.5 years (range: 50–75); however, BMI data were unavailable. Pre-preparation computed tomographic (CT) scans showed no bone hyperplasia or structural abnormalities as reviewed by two individual experts (SBY and HJS). Additionally, CT images of the left proximal femur from a healthy 45-year-old female volunteer (BMI 19.7, no chronic disease or fracture history) were included with informed consent for 3D reconstruction-based FEA.

P45 sectional plastination technique

The P45 sectional plastination technique was conducted at Dalian Hoffen Biotechnique Co. Ltd., China, following similar protocols from previous studies [24, 25]. Specimens were frozen at -70 °C, sliced into 3 mm sections, rinsed, bleached, dehydrated in acetone, impregnated with P45 polyester, and cured at 40 °C. Slices were prepared in coronal, sagittal, and transverse planes. Photographs of the slices were taken with a Canon EOS 7D Mark II camera against an LED illuminator, and all observations were documented accordingly (Fig. 1).

3D reconstruction and FEA

CT scan images were imported as non-strict DICOM files into Materialise Mimics (v. 19) for 3D reconstruction using segmentation and region growing tools, and into 3-Matic Research (v. 11) for surface and volume meshing, as well as material property assignment based on similar protocols from previous studies [1, 10]. The proximal femur was meshed using C3D4 elements (4-node tetrahedral linear solid elements) in Abaqus CAE 2020 (Dassault Systèmes). A mesh sensitivity analysis was performed until the maximum von Mises stress showed a negligible change (relative error < 5%). The final model had an element size of 1 mm. Mesh convergence was verified between 0.6 mm and 1 mm, showing a difference of less than 5%. The 3D model was then exported for FEA in Abaqus CAE 2020. A bipedal stance was assumed, with one-third (33%) of body weight distributed on each hip joint. Static and dynamic loads, based on Taylor et al. [9], were applied to the load-bearing areas of the proximal femur (Fig. 2) to assess compression and tension (Figs. 3 and 4). Material properties, volume and surface mesh values, convergence tests and load distribution data sets are given in the supplementary table.

Results

The morphology and pattern of all primary and secondary trabecular groups were examined in nine coronally sliced hips, with two images selected for description (Fig. 1A, B); seven superior transverse sectioned hips, with three images selected (Fig. 1C, D, F); and five sagittally sliced hips, with one image selected (Fig. 1E). Simplified illustrations of the corresponding frontal and superior transverse sections are provided in (Fig. 1G, H).

Morphology and pattern

Cortex

The cortex of the femoral neck was thinnest at the head-neck junction, particularly in the anterior superior quadrant and around the posterior aspect near Ward's triangle. It gradually thickened inferiorly along the medial border of the femoral shaft, forming the calcar femorale. The calcar descended anteroposteriorly and merged with the lesser trochanter (Fig. 1A, B and D).

Primary trabecular groups

A primary vertical group (PVG) of trabeculae originated from the medial border of the shaft from the calcar, extending from the middle diaphysis and attaching to the superomedial surface of the femoral head (Fig. 1A and B). These trabeculae were notably thick and densely packed, predominantly in the medial portions of the femoral neck and head, creating a unique mushroom pattern observed in frontal and superior transverse sections (Fig. 1A, B and F). This vertical group intersected with two distinct horizontal trabecular groups at the centre of the femoral head, near the epiphyseal scar, forming the medial trabecular system and the superomedial boundaries of Ward's triangle (Fig. 1A-D).

The first primary horizontal trabecular group (PHG 1) connected the femoral head to the femoral neck. It originated from the anterolateral and posterolateral aspects of the greater trochanter and the posterolateral wall of the femoral shaft. The trabeculae formed an arc through the femoral neck, with the majority of struts inserting into the anteromedial region, while the remainder merged with the second primary horizontal group (PHG 2) within the femoral head (Fig. 1A–E, G, H). The PHG 2 extended from the anterolateral aspect of the greater trochanter and the anterolateral wall of the femoral neck. It ran obliquely across the femoral head, connecting the posteromedial and anteromedial portions of the articular surface (Fig. 1C, D, H).

Secondary and small trabecular groups

Secondary trabecular groups within the trochanters and root of the neck mainly consisted of secondary vertical, horizontal, and oblique trabeculae, creating a complex lattice. The secondary vertical group (SVG) ascended from the medial calcar and extended superolaterally to the apex of the greater trochanter. It intersected with the primary and secondary horizontal trabeculae, forming the inferolateral boundary of Ward's triangle. The secondary horizontal group (SHG) originated from the posterolateral aspect of the greater trochanter and the lateral wall of the diaphysis, arcing within the neck-trochanteric junction and extending superomedially to cross the SVG and join the PHG 1 and PHG 2 (Fig. 1A, B, G, H). Oblique trabecular groups were observed within the apical part of the greater trochanter and the root of the femoral neck, merging with SVH and SHG (Fig. 1C, H). Together, these formed the lateral trabecular system at the neck-trochanteric junction (Fig. 1B-D).

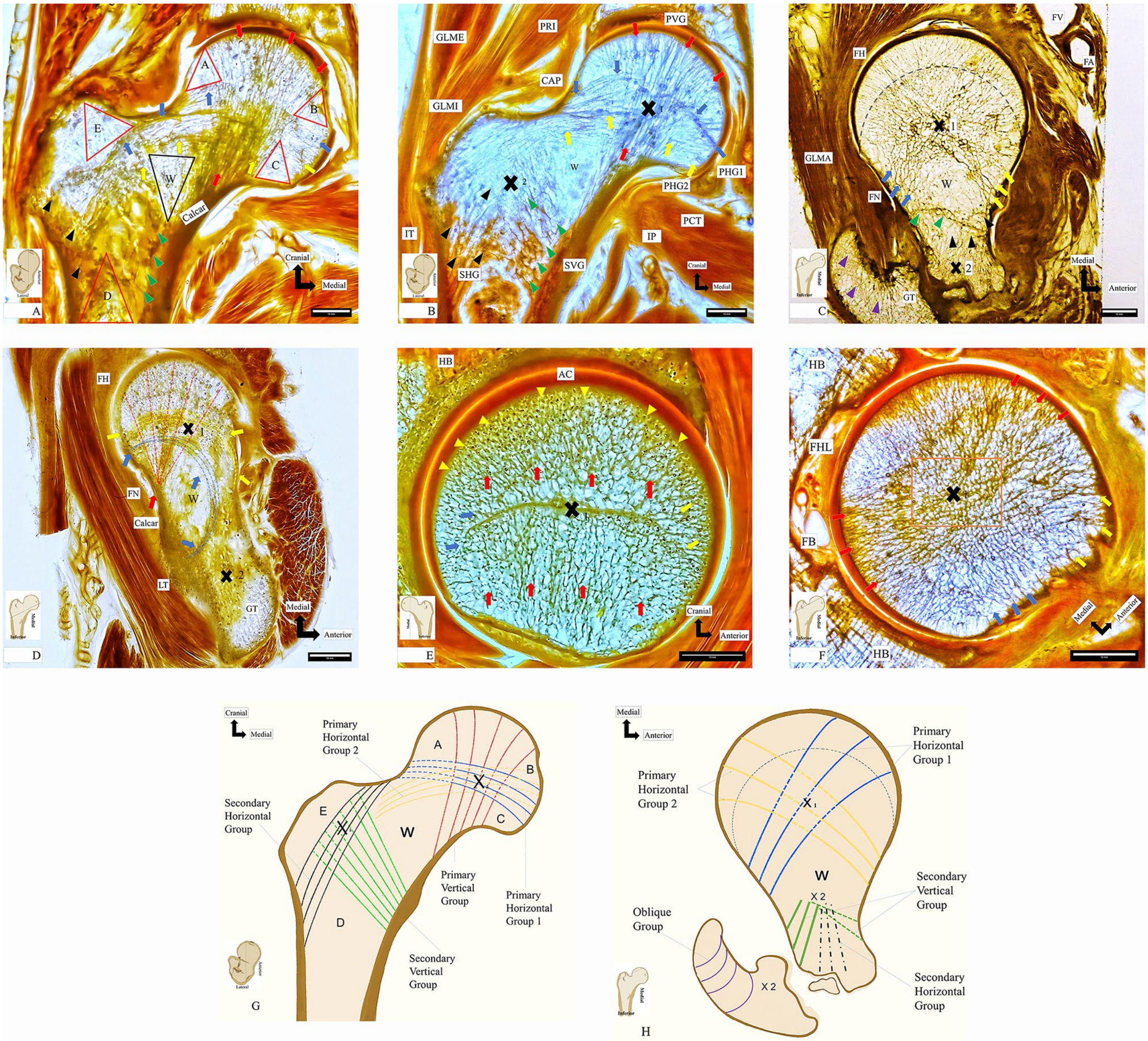

Fig. 1 P45 plastinated sections. Coronal sections (**A** and **B**): Triangles labelled **A**-**C** are seen in the FH, located between primary vertical and two primary horizontal groups. PHG 1 (blue arrows), PHG 2 (yellow arrows), and PVG (red arrows) are identified. Triangle **D** is seen in the diaphysis, located between SVG (small green triangles) and SHG (small black triangles). Triangle **E** is formed within the GT by the intersections of PHGs and the cortical contour of the GT. W represents Ward's triangle. The medial trabecular system (X1) is formed by the intersection of PVG, PHG 1 and PHG 2 in the FH, while the lateral trabecular system (X2) arises from the intersection of SVG and SHG within the FN, diaphysis, and GT. Superior transverse sections (**C** and **D**): The orientation, pattern, and extent of the two primary horizontal groups from the posterolateral (blue dotted lines and arrows; PHG 1) and anterolateral (yellow dotted lines and arrows; PHG 2) walls of the FN to the medial part of the FH, intersecting with the PVG (red dotted lines and arrows) to form the medial trabecular system (X1). SHG (small black triangles) and SVG (small green triangles) intersected at the neck-trochanteric junction, forming lateral trabecular system (X2). Oblique trabecular groups (small purple triangles) are observed in the posterior part of the GT. The black dotted line represents the epiphyseal scar. Medial sagittal section **(E)** and superior transverse section **(F)** of the FH: Area of formation (rectangle) of the medial trabecular system (X1) by the PHG 1 (blue arrows), PHG 2 (yellow arrows), and PVG (red arrows) merging in the centre of the FH. Trabecular struts align with the trabeculae of the hipbone. A fine meshwork of the subchondral trabecular network (small yellow triangles) is observed beneath the articular cartilage. **Bar: 10** mm. Illustrated diagrams of corresponding frontal **(G)** and superior transverse **(H)** sections of the proximal femur: PVG (red lines) is intersected by PHG 1 (blue lines), PHG 2 (yellow lines), forming the medial trabecular system (X1) in the FH. SVG (green lines), SHG (black dotted lines), and the oblique trabecular group (purple lines in the GT) form the lateral trabecular system (X2) in the femoral neck and trochanter. A–E represent potential triangular spaces between trabecular groups. W: Ward's triangle

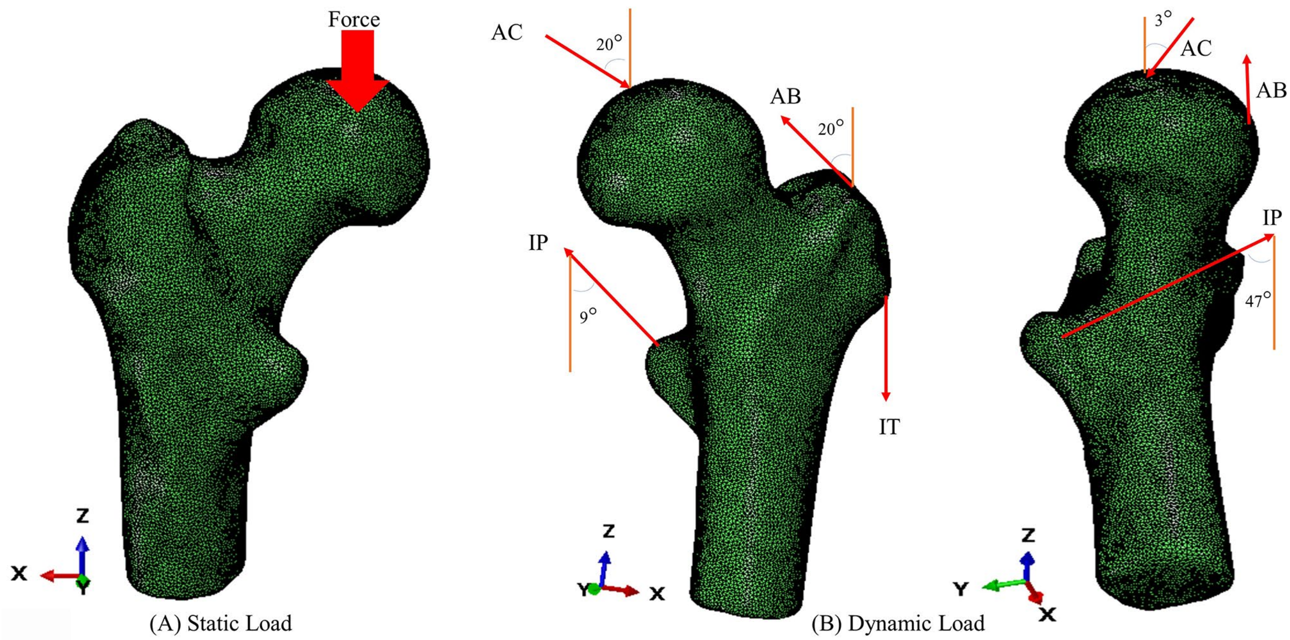

Fig. 2 3D reconstructed model with surface and volume mesh **(A)** static force (red arrow) on weight-bearing area of the femoral head **(B)** dynamic forces by acetabulum (AC) acted as compression, while forces produced by abductors (AB), iliotibial tract (IT), and iliopsoas (IP) follow their respective line of pull

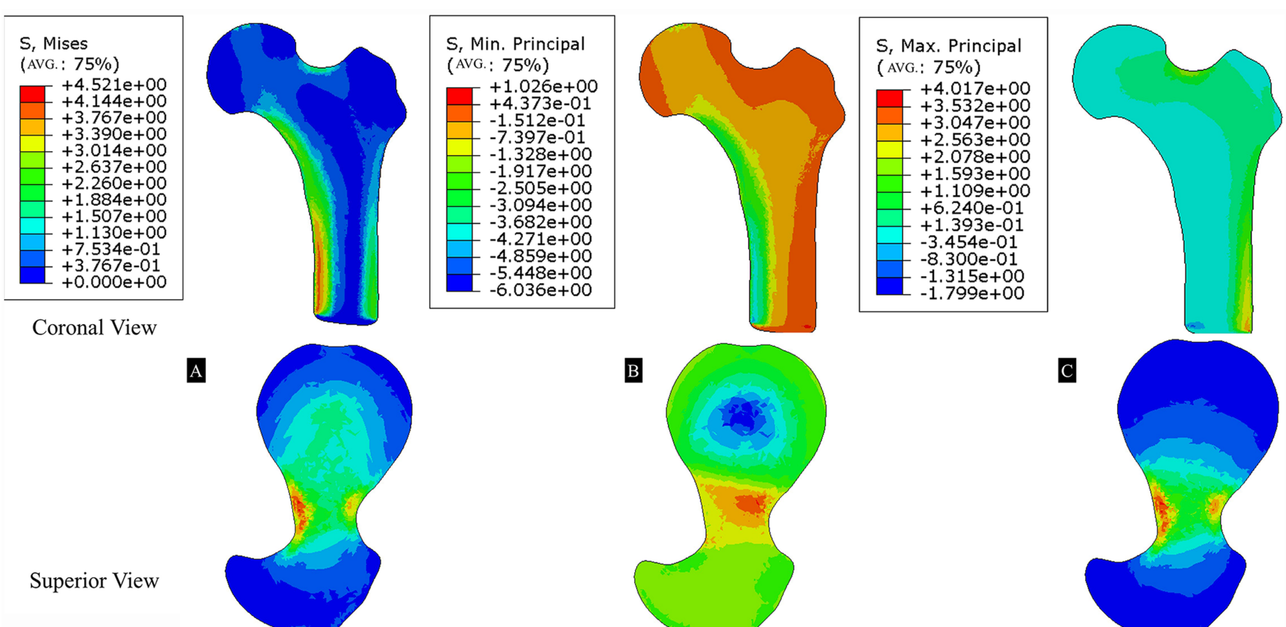

Fig. 3 Static load distribution in frontal and superior view; intensity from high to low (red to blue). **(A)** Von misses stress distribution to evaluate the level of deformity, **(B)** minimum principal stress distribution to evaluate compressive load, and **(C)** maximum principal stress distribution to evaluate tensile forces. All positives are tensile, and negatives are compressive forces in S, Max principal, and S, Min. principal. All numerical values in the boxes are in MPa

Small trabecular groups, consisting of subchondral trabeculae within the femoral head, were located just beneath the articular cartilage. These appeared as tightly packed, fine striations with a fan-like orientation, radiating from the articular surface into the deeper layers of trabecular bone and merging at the epiphyseal line (Fig. 1E and F). Moreover, the majority of these trabecular struts were aligned with trabecular struts of the hipbone (Fig. 1F).

The unique crossing pattern of these trabecular groups created six distinct triangular spaces. Five of these triangles have their bases along the cortex of the proximal femur, with their apices directed centrally, as clearly observed in frontal sections (Fig. 1A, G). The sixth

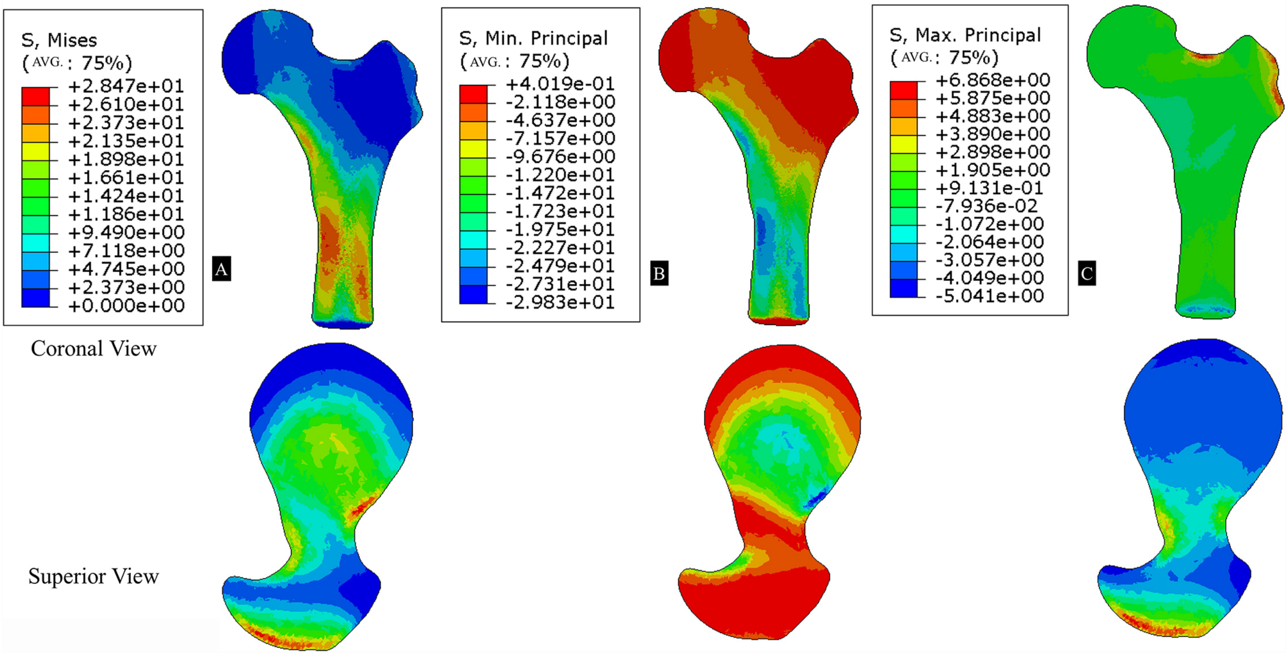

Fig. 4 Dynamic load distribution in frontal and superior view; intensity from high to low (red to blue). **(A)** Von misses stress distribution to evaluate the level of deformity, **(B)** minimum principal stress distribution to evaluate compressive load, and **(C)** maximum principal stress distribution to evaluate tensile forces. All positives are tensile, and negatives are compressive forces in S, Max principal, and S, Min. principal. All numerical values in the boxes are in MPa

triangular space, known as Ward's triangle, was located at the centre of the femoral neck and was bounded by the primary and secondary trabecular groups (Fig. 1A-D).

Stress test analysis

Static load

The stress distribution during bipedal standing illustrated the natural flow of load within the bone (Fig. 2A). The medial border of the femoral shaft, including the calcar, and the anterolateral and posterolateral walls of femoral neck exhibited the highest deformative stress (Von Mises Stress, 1.130e + 00 to 4.521e + 00 MPa). Maximum compression was observed in the primary load-bearing areas of the femoral head under the lunate surface of the acetabulum, along the PVG, the medial border of the femoral shaft with the calcar, and at the base of both trochanters (Min. Principal Stress, -6.036e + 00 to -1.917e + 00 MPa). Maximum tensile stress was observed throughout the femoral neck, particularly along the anterolateral and posterolateral walls, corresponding to the PHG 1 and PHG 2, the greater trochanter, and the lateral border of the femoral shaft (Max. Principal Stress, 1.109e + 00 to 4.017e + 00 MPa), as shown in Fig. 3.

Dynamic load

The dynamic load represented the compressive forces exerted by the acetabulum (AC) and the pull of the iliotibial tract (IT), iliopsoas (IP), and abductor muscles (AB), as shown in Fig. 2B. Maximum deformative stress was concentrated along the medial border of the femoral shaft, including the calcar, the anterolateral wall of the femoral neck, the apex of the greater trochanter, and the cortex of the diaphysis (Von Mises Stress, 7.118e + 00 to 2.8471e + 01 MPa). Maximum compression occurred along the PVG, directed toward the diaphysis (Min. Principal Stress, -2.983e + 01 to -4.637e + 00 MPa). Maximum tensile stress was distributed from the femoral head and neck, along the PHG 1 and PHG 2, extending to the greater trochanter and the lateral border of the femoral shaft (Max. Principal Stress, 9.131e-01 to 6.868e + 00 MPa), as shown in Fig. 4.

Discussion

This study examines the morphology, distribution, and spatial relationships of trabecular groups in the human proximal femur using P45 plastinated coronal, sagittal, and transverse sections. P45 sectional plastination is an innovative technique that produces thin, transparent anatomical slices while preserving spatial details with incomparable accuracy. Unlike conventional dissections, radiological imaging, or histological techniques, which are often prone to artefacts and structural distortions, P45 plastination maintains the natural colouration of tissues, enhancing morphological fidelity. However, a key limitation of this method is its inability to visualise intraosseous neurovascular structures, necessitating complementary techniques for a more comprehensive assessment.

To further investigate the biomechanical function of trabecular architecture, 3D reconstruction-based FEA of a living human subject was employed to evaluate load distribution, particularly compression and tension patterns within the trabecular groups. This integrated approach provides a simple yet comprehensive understanding of the functional morphology of trabecular bone in the proximal femur. The findings of this study have important implications for optimising surgical techniques and improving the design of orthopaedic implants, contributing to advancements in clinical applications.

Load adaptation in the proximal femur

The complex morphology and functional adaptation of the proximal femoral trabecular bone are critical for load-bearing and overall hip biomechanics [2, 6]. As demonstrated in the results section, the primary and secondary trabecular groups, located in the femoral head, neck and trochanters, are firmly integrated with the outer cortical bone, forming a unique lattice. This anatomical arrangement is vital for effective load distribution and stress transfer during both static and dynamic activities. During bipedal stance, compressive load was mainly distributed through cortical bone, calcar femorale, and trabeculae in a downward direction. FEA revealed that most of the load was transferred from the cortical bone to cancellous bone, primarily in the femoral head, which shifted to the neck and intertrochanteric region. These observations aligned with studies performed by Lotz et al. [26], and Nawathe et al. [27]. The findings support Wolff's law, which suggests that the trabecular architecture adapts to mechanical loading [12, 13]. Additionally, our results are also consistent with recent studies [14–16, 28], indicating that trabecular function is not solely determined by stress trajectories but also influenced by interaction with cortical bone and soft tissues. This highlights the complex nature of trabecular adaptation, where both internal and external forces contribute to bone strength and stability.

Trabecular architecture and load stabilization

The results revealed that the femoral head and neck possess unique horizontal and vertical trabecular groups, forming a dynamic support system that stabilises the femoral shaft. The dense primary vertical group, originating from the calcar femorale and radiating toward the superior articular surface, provides primary support during standing and walking. P45 sections revealed this group to be mushroom-shaped, with the stalk originating from the calcar and supporting the cap at centre of the femoral head (Fig. 1A, B, E, and F). This finding aligns with a recently published P45 plastinated study by Zhang et al., [24] and differs from previous CT imaging-based descriptions of the group as dumbbell-shaped and hemispheric [21, 22].

Meanwhile, two distinct primary horizontal groups played a crucial role in managing tensile forces, particularly along the anterolateral and posterolateral walls of the femoral neck. Previously, the structure was believed to be a single, unified trabecular column [7, 10, 11]. However, P45 plastinated sections have revealed two distinct groups of primary horizontal trabeculae with different origins, patterns, and attachments [24]. By counterbalancing vertical support and resisting shear tensile forces, these horizontal trabeculae contributed to the overall stability of the bone under multidirectional loading. This is consistent with Kim et al. [28], and Zhang, Li, et al. [10], but differs from Hammer [7], who described horizontal trabeculae primarily resisting compressive rather than tensile forces. Furthermore, the anterolateral and posterolateral areas of the femoral neck, corresponding to the apex of the primary horizontal groups, exhibited peak deformity values in von Mises stress under both static and dynamic loads. Kim et al. [28], also quantitatively analysed strain energy density and identified maximum stress in these specific regions. Additionally, Wang et al. [2], reported that these regions are more prone to osteoporotic fractures. Therefore, anterolateral and posterolateral areas of the femoral neck are considered vulnerable zones for femoral neck fractures, particularly in osteoporotic bones. Collectively, these trabecular groups formed the medial trabecular system, enhancing structural resilience against medial bending forces and facilitating load distribution across the femoral head, especially during movements that induced shear stresses.

Likewise, the lateral trabecular system provides added support in managing tensile forces along the femur's outer regions, resisting lateral bending forces and enhancing stability during movement. Anatomically this system is located in the greater trochanter and intertrochanteric region (Fig. 1B, C). Wang et al. [2], and Lindskog and Baumgaertner [29], revealed that these regions are under shear forces, with the highest number of fractures occurring in the elderly, most of which are unstable. In the present study, these regions are identified as vulnerable zones for intertrochanteric and avulsion fractures due to the strong upward pull of the hip abductors and the downward pull of the iliotibial tract (Figs. 1B and C and 2B). These forces are particularly impactful in osteoporotic bone, where reduced bone density compromises structural integrity [30]. Moreover, the oblique trabecular group, in combination with the secondary vertical group, resists the pulling forces from the gluteal muscles, thereby further strengthening the greater trochanter [11, 22]. Similarly, the subchondral trabeculae beneath articular cartilage of the femoral head provide a firm shock-absorbing system that resists deformation, supporting articular cartilage and reducing the risk of degenerative diseases like osteonecrosis of the femoral head (ONFH)

[28, 31]. These observations are consistent with recent load distribution models described in radiological and biomechanical studies [6, 8, 10].

Triangular spaces and vascular dynamics in the proximal femur

The triangular spaces of the proximal femur, formed by intersecting trabecular groups, are essential for biomechanical integrity, vascular supply, and overall bone health. Studies have revealed that intraosseous epiphyseal arteries divide into small branches at the superior, middle, and inferior parts of the femoral head, anatomically correspond to these triangular spaces to supply the trabecular and subchondral bone, and support cartilage health [20, 32]. Damage to this delicate vascular network can lead to avascular necrosis (AVN) and ONFH [33–35]. Similarly, the triangular spaces in the greater trochanter and diaphysis accommodate the blood vessels supplying their respective regions. These spaces likely accommodate intraosseous microcirculation during high-intensity activities. A comparative anatomical study by Shah et al. [20, 23], revealed an inverse correlation between trabecular density and vascularity in the proximal femur of canines, with higher trabecular density being associated with lower vascularity. This warrants further investigation in humans, focusing on dynamic microcirculation, to provide additional insights into this relationship.

In addition, Ward's triangle serves as a diagnostic indicator of bone quality and strength in clinical settings. Its widening has been associated with an increased fracture risk in osteoporosis [8], while its adaptability to mechanical loads highlights its role in load transmission [6]. The P45 plastinated sections revealed that the superomedial boundary is formed by the primary vertical group and two primary horizontal groups, while the inferolateral boundary is formed by the secondary vertical group (Fig. 1A, G, H). Ultimately, the medial and lateral trabecular systems are separated by Ward's triangle. FEA suggests that its medial boundary primarily accommodates compressive forces, while the superior and lateral boundaries manage tensile forces. These observations clarify the precise trabecular boundaries, their functions, and the location of this structure, further expanding the descriptions provided in previous studies [6–8, 11, 24, 36]. Therefore, implants designed to align with the trabecular framework of these spaces could enhance integration, stability, and load distribution.

Optimizing proximal femoral implants

Existing proximal femoral implants, such as the Corail hip stem, Exeter femoral stem, and proximal femoral locking plates (PFLP), are designed to restore biomechanical function but have notable limitations [1, 37, 38]. A major issue is stress shielding, caused by the stiffness mismatch between the implant and native bone, which leads to adaptive bone resorption and compromises long-term stability [4, 5, 39]. Moreover, these implants may not fully replicate the anisotropic mechanical properties and trabecular microarchitecture of the proximal femur, resulting in suboptimal load distribution and altered stress trajectories [16, 37, 38]. Recent studies on implant-bone interactions have shown that traditional implants, primarily designed to manage compressive forces only, can disrupt the natural trabecular pattern, leading to stress shielding, implant loosening, and delayed healing [3, 4, 16].

Clinical reports on recently developed proximal femoral bionic nails (PFBN) to treat intertrochanteric fractures have shown promising effects in fracture healing and early recovery [30, 40]. However, they also have shortcomings, such as prolonged operation time and the unfamiliar location of their supporting screws [30], highlighting the need for further design refinement. Given that the trabecular architecture of the proximal femur handles complex forces, PFBN design should account for both compressive and tensile stresses while preserving the trabecular anatomy. Areas of maximum stress, such as Ward's triangle, the intertrochanteric region, the subtrochanteric region, and the greater trochanter, which contains the lateral trabecular system and the pathway of the primary horizontal groups, are particularly vulnerable. These areas represent critical targets for enhancing PFBN designs to minimise stress shielding and improve bone-implant integration [1, 3].

Based on the anatomical and biomechanical observations of trabeculae in current study, refinements in implant design are suggested to prioritise targeted screw placement to minimise excessive drilling. Focus is recommended on areas with high calcar strength and optimal cancellous bone density, such as the intersections of medial and lateral trabecular systems. Likewise, slight adjustments in the angle and location of supporting screws to preserve the inferolateral boundary of Ward's triangle are advised. Additionally, materials with elastic properties similar to bone, combined with porous or bioactive surfaces, are proposed to enhance osseointegration, particularly in osteoporotic patients [5]. Preserving the natural trabecular distribution is also equally important for vascularisation and efficient load transfer.

To reduce biomechanical inefficiencies, advanced designs, such as 3D-printed trabecular metal implants and biomimetic femoral stems, integrate lattice structures and finite element-driven optimisation to enhance physiological load transfer and improve bone-implant interface mechanics [16, 41, 42]. Patient-specific 3D-printed implants have the potential to replicate trabecular architecture, providing a biomechanically optimised solution for orthopaedic procedures [42, 43]. Utilising additive manufacturing techniques such as selective laser melting (SLM) or electron beam melting (EBM), these implants can be personalised to match a patient's bone morphology and mechanical properties [42, 44]. Moreover, these implants feature controlled porosity to support vascular infiltration, osteointegration, and load distribution. By mimicking the anisotropic mechanical behaviour of native trabeculae, they optimise load transfer, reduce stress shielding, and lower the risk of implant loosening and periprosthetic bone loss [42]. Computational modelling, including the FEA, further refines their design for optimal biomechanical compatibility [45].

Further studies are needed to establish standardised reporting of clinical outcomes and to explore the long-term efficacy and safety of these implants [45, 46]. These advancements can significantly lower the risk of implant failure and reduce the need for revision surgeries, ultimately improving long-term patient outcomes. Future research should focus on elucidating vascular distribution within the trabecular part of the proximal femur to further optimise surgical techniques and implant designs.

Limitations

This study has several limitations. The trabecular architecture was not analysed with respect to sex, occupation, race, or age. Due to the small sample size, the data cannot be generalised to a broader population. Moreover, quantitative morphology was not included. Additionally, the assumptions for the FEA model under static and dynamic loads were simplified, and extreme conditions such as jumping, running, stretching, or ligament support, which are relevant to certain clinical scenarios, were not simulated. Despite these limitations, the current study provides a novel perspective on the functional morphology of the proximal femoral trabecular system in a systematic and simplified manner. Future studies will incorporate morphometric and 3D reconstruction-based FEA of trabeculae and intraosseous blood vessels to optimise surgical techniques.

Conclusion

The human proximal femur comprises medial and lateral trabecular systems, formed by primary and secondary trabecular groups, essential for resisting medial and lateral bending forces. The primary horizontal trabeculae, consisting of two distinct groups, play a key role in managing tensile forces along with the secondary horizontal group, while the primary vertical group handles compression. Secondary vertical and oblique groups counteract muscular loads at the greater trochanter, whereas small trabecular groups maintain the contour of the femoral head. The strength of the proximal femur relies on dense cortical bone, the calcar femorale, trabecular systems, and the greater trochanter. Potential weak zones, including Ward's triangle, the intertrochanteric region, and the anterolateral and posterolateral walls of the femoral neck, serve as key pathways for primary horizontal trabeculae managing shear bending forces during static and dynamic loads. PFBN and patient-specific 3D-printed implants should align with these physiological load patterns, reconstructing both compressive and tensile trabecular groups to reduce post-operative complications. Integrating these insights into clinical practice can improve long-term outcomes for patients undergoing hip arthroplasty, particularly those with osteoporosis.

Abbreviations

ONFH	Osteonecrosis of the Femoral Head
CT	Computed Tomography
AB	Abductor Muscles
AC	Articular Cartilage
CAP	Capsule of Hip Joint
FA	Femoral Artery
FB	Foveal Blood Vessels
FH	Femoral Head
FHL	Femoral Head Ligament
FN	Femoral Neck
FV	Femoral Vein
GLMA	Gluteus Maximus
GLME	Gluteus Medius
GLMI	Gluteus Minimus
GT	Greater Trochanter
HB	Hip Bone
IP	Iliopsoas
IT	Iliotibial Tract
LT	Lesser Trochanter
PCT	Pectineus
PRI	Piriformis
FEA	Finite Element Analysis
PFBN	Proximal Femoral Bionic Nail
AVN	Avascular Necrosis
MPa	Megapascal
SLM	Selective Laser Melting
EBM	Electron Beam Melting
PFLP	Proximal Femoral Locking Plates
PVG	Primary Vertical Group
PHG	Primary Horizontal Group
SVG	Secondary Vertical Group
SHG	Secondary Horizontal Group

Supplementary Information

The online version contains supplementary material available at https://doi.org/10.1186/s13018-025-05773-5.

Supplementary Material 1

Acknowledgements

The authors thank all participants and funding authorities. We are grateful to Cheng Chen, Zhi-Jun Zhang, Qi Ying, Ze-Long Li, and Chen-Yi Gan for assisting with gross dissection at Dalian Medical University. Additionally, we acknowledge Ruan Zhang-Kun, Zhao Long-Shi, and Chen Zhi-Gang at Dalian Hoffen Biotechnique Company Ltd., Dalian, China, for providing technical support for the specimen preservation and P45 sectional plastination.

Author contributions

MAAS: writing– original draft, visualisation, methodology, investigation, formal analysis, data curation, conceptualisation. SJL: formal analysis, methodology, data curation, resources, software. JFZ: methodology, investigation, resources, data curation. JWW: investigation, formal analysis, data curation. WT:

validation, methodology, investigation, formal analysis. WCL: investigation, methodology, data curation. HXL: investigation, formal analysis, data curation. SBY: conceptualisation, supervision, formal analysis, funding acquisition, resources. HJS: conceptualisation, writing– original draft, revising & editing, supervision, visualisation, conceptualisation, formal analysis.

Funding
This study was supported by the Key R&D Project of Liaoning Province (2020JH/1050004).

Data availability
No datasets were generated or analysed during the current study.

Declarations

Ethical approval
This study was approved by the Biomedical Ethics Committee of Dalian Medical University (Ethics number: 2023-004). All cadavers were provided by the Department of Anatomy, Dalian Medical University, China.

Consent for publication
Not applicable.

Declaration of generative AI and AI-assisted technologies in the writing process
No AI was used to analyse or describe data.

Competing interests
The authors declare no competing interests.

Author details
[1]Department of Anatomy, College of Basic Medicine, Dalian Medical University, 9 West Section, Lushun South Road, Dalian 116044, People's Republic of China

Received: 21 February 2025 / Accepted: 31 March 2025
Published online: 12 April 2025

References

1. Cun Y, Dou C, Tian S, Li M, Zhu Y, Cheng X, et al. Traditional and bionic dynamic hip screw fixation for the treatment of intertrochanteric fracture: a finite element analysis. Int Orthop. 2020;44(3):551–9. https://doi.org/10.1007/s00264-019-04478-9.
2. Wang H, Zhang Y, Ren C, Ding K, Zhang Q, Zhu Y, et al. Biomechanical properties and clinical significance of cancellous bone in proximal femur: A review. Injury. 2023. https://doi.org/10.1016/j.injury.2023.03.010.
3. Cheng X, Yang Y, Zhu J, Li G, Chen W, Wang J, et al. Finite element analysis of basicervical femoral neck fracture treated with proximal femoral bionic nail. J Orthop Surg Res. 2023;18(1):926. https://doi.org/10.1186/s13018-023-04415-y.
4. Liu B, Wang H, Zhang M, Li J, Zhang N, Luan Y, et al. Capability of auxetic femoral stems to reduce stress shielding after total hip arthroplasty. J Orthop Translation. 2023;38:220–8. https://doi.org/10.1016/j.jot.2022.11.001.
5. Zhang Q, Chen Z, Peng Y, Jin Z, Qin L. The novel magnesium-titanium hybrid cannulated screws for the treatment of vertical femoral neck fractures: Biomechanical evaluation. J Orthop Translation. 2023;42:127–36. https://doi.org/10.1016/j.jot.2023.08.003.
6. Xu G, Li J, Xu C, Xiong D, Li H, Wang D, et al. Triangular mechanical structure of the proximal femur. Orthop Surg. 2022;14(11):3047–60. https://doi.org/10.1111/os.13498.
7. Hammer A. The structure of the femoral neck: A physical dissection with emphasis on the internal trabecular system. Annals Anat - Anatomischer Anzeiger. 2010;192(3):168–77. https://doi.org/10.1016/j.aanat.2010.02.007.
8. Ding K, Zhu Y, Li J, Yuwen P, Yang W, Zhang Y, et al. Age-related changes with the trabecular bone of Ward's triangle and Neck-shaft angle in the proximal femur: A radiographic study. Orthop Surg. 2023;15(12):3279–87. https://doi.org/10.1111/os.13923.
9. Taylor ME, Tanner KE, Freeman MA, Yettram AL. Stress and strain distribution within the intact femur: compression or bending? Med Eng Phys. 1996;18(2):122–31. https://doi.org/10.1016/1350-4533(95)00031-3.
10. Zhang J, Li H, Zhou Y, Chen S, Rong Q. An analysis of trabecular bone structure based on principal stress trajectory. Bioengineering. 2023;10(10). https://doi.org/10.3390/bioengineering10101224.
11. Skuban TP, Vogel T, Baur-Melnyk A, Jansson V, Heimkes B. Function-orientated structural analysis of the proximal human femur. Cells Tissues Organs. 2009;190(5):247–55. https://doi.org/10.1159/000210065.
12. Pearson OM, Lieberman DE. The aging of Wolff's law: ontogeny and responses to mechanical loading in cortical bone. Am J Phys Anthropol 2004;Suppl 39:63–99 https://doi.org/10.1002/ajpa.20155
13. Wolff J. Das gesetz der transformation der Knochen. Dtsch Med Wochenschr. 1893;19(47):1222–4. https://doi.org/10.1055/s-0028-1144106.
14. Kivell TL. A review of trabecular bone functional adaptation: what have we learned from trabecular analyses in extant hominoids and what can we apply to fossils? J Anat. 2016;228(4):569–94. https://doi.org/10.1111/joa.12446.
15. Tsegai ZJ, Skinner MM, Pahr DH, Hublin JJ, Kivell TL. Systemic patterns of trabecular bone across the human and chimpanzee skeleton. J Anat. 2018;232(4):641–56. https://doi.org/10.1111/joa.12776.
16. Ding Z, Wang J, Wang Y, Zhang X, Huan Y, Zhang D. Bionic reconstruction of tension trabeculae in short-stem hip arthroplasty: a finite element analysis. BMC Musculoskelet Disord. 2023;24(1):89. https://doi.org/10.1186/s12891-023-06205-3.
17. Ogut E. Is the third trochanter of the femur a developmental anomaly, a functional marker, or an evolutionary adaptation? Canadian society of forensic. Sci J. 2023;56(3):123–42. https://doi.org/10.1080/00085030.2022.2104563.
18. Ascenzi MG, Hetzer N, Lomovtsev A, Rude R, Nattiv A, Favia A. Variation of trabecular architecture in proximal femur of postmenopausal women. J Biomech. 2011;44(2):248–56. https://doi.org/10.1016/j.jbiomech.2010.10.017.
19. Saers JPP, DeMars LJ, Stephens NB, Jashashvili T, Carlson KJ, Gordon AD, et al. Combinations of trabecular and cortical bone properties distinguish various loading modalities between athletes and controls. Am J Phys Anthropol. 2021;174(3):434–50. https://doi.org/10.1002/ajpa.24176.
20. Shah MAA, Tang W, Zhang J-H, Chen C, Wang J-W, Lü S-J, et al. Microvasculature and trabecular bone in beagle proximal femur: microstructural insights. Annals Anat - Anatomischer Anzeiger. 2025;258:152368. https://doi.org/10.1016/j.aanat.2024.152368.
21. Stiehl JB, Jacobson D, Carrera G. Morphological analysis of the proximal femur using quantitative computed tomography. Int Orthop. 2007;31(3):287–92. https://doi.org/10.1007/s00264-006-0182-z.
22. Elke RP, Cheal EJ, Simmons C, Poss R. Three-dimensional anatomy of the cancellous structures within the proximal femur from computed tomography data. J Orthop Res. 1995;13(4):513–23. https://doi.org/10.1002/jor.1100130406.
23. Shah MAA, Tang W, Ma Y, Zhe W, Yu SB, Sui HJ. Regional distribution of microvasculature within the canine femoral head: a study of plastinated tissue histology and 3D reconstruction. J Orthop Surg Res. 2025;20(1):170. https://doi.org/10.1186/s13018-025-05522-8.
24. Zhang JF, Lü SJ, Wang JW, Tang W, Li C, Campbell G, et al. The qualitative analysis of trabecular architecture of the proximal femur based on the P45 sectional plastination technique. J Anat. 2025. https://doi.org/10.1111/joa.14210.
25. Cheng J, Alam Shah MA, Wang J-W, Jiang W-B, Zhang X-H, Sui H-J, et al. Anterior attachments of the medial patellofemoral ligament: morphological characteristics. J Bone Joint Surg. 2025. https://doi.org/10.2106/JBJS.24.00332.
26. Lotz JC, Cheal EJ, Hayes WC. Stress distributions within the proximal femur during gait and falls: implications for osteoporotic fracture. Osteoporos Int. 1995;5(4):252–61. https://doi.org/10.1007/bf01774015.
27. Nawathe S, Nguyen BP, Barzanian N, Akhlaghpour H, Bouxsein ML, Keaveny TM. Cortical and trabecular load sharing in the human femoral neck. J Biomech. 2015;48(5):816–22. https://doi.org/10.1016/j.jbiomech.2014.12.022.
28. Kim J, Chun BJ, Kim JJ. Quantitative load dependency analysis of local trabecular bone microstructure to understand the Spatial characteristics in the synthetic proximal femur. Biology. 2023;12(2). https://doi.org/10.3390/biology12020170.
29. Lindskog DM, Baumgaertner MR. Unstable intertrochanteric hip fractures in the elderly. J Am Acad Orthop Surg. 2004;12(3):179–90. https://doi.org/10.5435/00124635-200405000-00006.
30. Duan W, Liang H, Fan X, Zhou D, Wang Y, Zhang H. Research progress on the treatment of geriatric intertrochanteric femur fractures with proximal femur

bionic nails (PFBNs). Orthop Surg. 2024;16(10):2303–10. https://doi.org/10.1111/os.14134.
31. Wang P, Wang C, Meng H, Liu G, Li H, Gao J, et al. The role of structural deterioration and Biomechanical changes of the necrotic lesion in collapse mechanism of osteonecrosis of the femoral head. Orthop Surg. 2022;14(5):831–9. https://doi.org/10.1111/os.13277.
32. Qiu X, Shi X, Ouyang J, Xu D, Zhao D. A method to quantify and visualize femoral head intraosseous arteries by micro-CT. J Anat. 2016;229(2):326–33. https://doi.org/10.1111/joa.12475.
33. Qiu X, Cheng L, By WBL, Yang L, Yu M, et al. Micro perfusion and quantitative analysis of the femoral head intraosseous artery. Orthop Surg. 2018;10(1):69–74. https://doi.org/10.1111/os.12364.
34. Zhao D, Wang Z, Cheng L, Tian S, Liu B, Yang L, et al. The significance of evaluating the femoral head blood supply after femoral neck fracture: a new classification for femoral neck fractures. Orthop Surg. 2022;14(4):742–9. https://doi.org/10.1111/os.13241.
35. Konarski W, Poboży T, Śliwczyński A, Kotela I, Krakowiak J, Hordowicz M, et al. Avascular necrosis of femoral head—overview and current state of the Art. Int J Environ Res Public Health. 2022;19(12):7348. https://doi.org/10.3390/ijerph19127348.
36. Lu Y, Wang L, Hao Y, Wang Z, Wang M, Ge S. Analysis of trabecular distribution of the proximal femur in patients with fragility fractures. BMC Musculoskelet Disord. 2013;14:130. https://doi.org/10.1186/1471-2474-14-130.
37. Wang Y, Chen W, Zhang L, Xiong C, Zhang X, Yu K, et al. Finite element analysis of proximal femur bionic nail (PFBN) compared with proximal femoral nail antirotation and intertan in treatment of intertrochanteric fractures. Orthop Surg. 2022;14(9):2245–55. https://doi.org/10.1111/os.13247.
38. Viberg B, Rasmussen K, Overgaard S, Rogmark C. Poor relation between Biomechanical and clinical studies for the proximal femoral locking compression plate. Acta Orthop. 2017;88:427–33. https://doi.org/10.1080/17453674.2017.1304207.
39. Kim JW, Oh CW, Kim BS, Jeong SL, Jung GH, Lee DH. Structure-mechanical analysis of various fixation constructs for basicervical fractures of the proximal femur and clinical implications; finite element analysis. Injury. 2023;54(2):370–8. https://doi.org/10.1016/j.injury.2022.12.004.
40. Zhao H, Deng X, Liu W, Chen W, Wang L, Zhang Y, et al. Proximal femoral bionic nail (PFBN)-an innovative surgical method for unstable femoral intertrochanteric fractures. Int Orthop. 2023;47(4):1089–99. https://doi.org/10.1007/s00264-023-05696-y.
41. Singh AP, Rana M, Pal B, Datta P, Majumder S, Roychowdhury A. Patient-specific femoral implant design using metamaterials for improving load transfer at proximal-lateral region of the femur. Med Eng Phys. 2023;113:103959. https://doi.org/10.1016/j.medengphy.2023.103959.
42. Okolie O, Stachurek I, Kandasubramanian B, Njuguna J. 3D printing for hip implant applications: A review. Polymers. 2020;12. https://doi.org/10.3390/polym12112682.
43. Wong K. 3D-printed patient-specific applications in orthopedics. Orthop Res Reviews. 2016;8:57–66. https://doi.org/10.2147/ORR.S99614.
44. Majumdar T, Eisenstein N, Frith J, Cox S, Birbilis N. Additive manufacturing of titanium alloys for orthopedic applications: A materials science viewpoint. Adv Eng Mater. 2018;20. https://doi.org/10.1002/adem.201800172.
45. Mitra I, Bose S, Dernell W, Dasgupta N, Eckstrand C, Herrick J, et al. 3D printing in alloy design to improve biocompatibility in metallic implants. Mater Today. 2021;45:20–34. https://doi.org/10.1016/J.MATTOD.2020.11.021.
46. Burnard J, Parr W, Choy W, Walsh W, Mobbs R. 3D-printed spine surgery implants: a systematic review of the efficacy and clinical safety profile of patient-specific and off-the-shelf devices. Eur Spine J. 2019;29:1248–60. https://doi.org/10.1007/s00586-019-06236-2.

Publisher's note